# Trust Characteristics of Ducted Fan of a Quadcopter in Various Flight Modes

Pavel Bulat and Pavel Chernyshov *

Posted Date: 26 March 2026

doi: 10.20944/preprints202603.2079.v1

Keywords: quadcopter; ducted fan; computational fluid dynamics; thrust; power

 doi:10.20944/preprints202603.2079.v1



*Article*

# Trust Characteristics of Ducted Fan of a Quadcopter in Various Flight Modes

**Pavel Bulat and Pavel Chernyshov ***

Research Laboratory "Flight Dynamics and Control of Unmanned Aircraft Systems", Federal State Autonomous Educational Institution of Higher Education "Sevastopol State University" Sevastopol, 299053, Russia

* Correspondence: pashachp8@gmail.com

**Abstract**

Ducted fans are widely used in vehicles that have high engine power per area. They are swept by the propellers of hovercraft and vertical take-off aircraft. Computational fluid dynamics is a powerful tool to select the aerodynamic configuration of new aircraft and engines, and to determine their optimal operating conditions. Full Navier–Stokes equations are used to simulate the airflow induced by the rotating blades of quadcopter props. The thrust characteristics of ducted fans are analyzed based on numerical simulations in different flight modes, such as hovering and oblique air flow. Tip clearance and inner wall effects on thrust and power are reported.

**Keywords:** quadcopter; ducted fan; computational fluid dynamics; thrust; power

## 1. Introduction

To ensure the effective operation of UAVs (unmanned aerial vehicles) in various modes of flight, it is necessary to solve a number of issues related to improving the aerodynamics of aircraft and their various components during the design phase. In particular, it is important to determine the characteristics of trust and the influence of propellers on other parts of UAV [1]. The results of numerical and experimental research show that propeller operation has a significant effect on aerodynamic forces, torque, and other characteristics [2,3]. Registration and processing of acoustic signals are used to identify aircraft of a certain class and their maneuvers, as well as to extract information useful for tracking location and movement [4,5].

Among potential small-size transport aircraft, a new type of relatively small multirotor aircraft has been developed - quadcopters. They have several advantages over other aircraft, such as compactness, maneuverability and low takeoff weight with significant payload [6]. Placing a fan in a duct can increase the propeller's thrust by up to 40% and reduce inductive losses on the blade tip. This leads to increased efficiency of the prop and decreased noise [7]. Additional thrust decreases with increasing speed of oncoming flow, so the ducted-fan is used as a main engine up to speeds no more than 150-180km The ability to generate high power with limited swept area makes ducted fans promising for aircraft with short takeoff and vertical landing.

One of the tools for optimizing the characteristics of new UAVs is numerical simulation using modern approaches to describing stationary and unsteady flow. This approach not only reduces costs at the initial design stage, but it also allows for the search for new shapes of UAVs. It is not only possible to calculate trust characteristics, but it is also possible to study the flow created by the propeller, which improves aerodynamic performance, allowing for increased flight speed, reduced fuel consumption, and improved stability and control of the aircraft.

A method for determining the nonlinear aerodynamic characteristics under non-stationary conditions is developed in [8]. The results of the experimental study of the aerodynamics of a model disk-shaped unmanned aerial vehicle with a rotor-in-a-ring support system (ducted fan, ducted/shrouded propeller) are presented in [9]. Research on the ducted fan is carried out both experimentally [10–13]

 doi:10.20944/preprints202603.2079.v1



and numerically, including the RANS/URANS approaches [14–17] and eddy - resolving approaches to modeling turbulent flows [18]. A review of the experimental and numerical research is presented in [19].

Eddy-resolving methods for modeling turbulent flows (DES) are used to solve the problem of calculating aeroelastic deformations of fan blades in [20]. Improving aerodynamic and acoustic characteristics of quadcopters is associated with finding optimal blade shapes. The difficulty of simulating aerodynamic characteristics in ducted fans in different flight modes depends on the operating conditions of propellers in profiled ducts and the flow around UAVs [21–25].

The difference in the nature of flow around a ducted fan during cruising flight and near-hovering modes requires studying the performance of propellers at various impingement angles and outside flow speeds [26]. In the presence of ground, a low-altitude aircraft is affected by strong vortices reflecting from the ground, leading to irregular impacts on aircraft structures [27,28].

The use of ducted double-row counter-rotating fans allows greater power to be extracted from the duct area [29]. The behavior of propellers in high pressure thrusters under moderate load (average blade angle is 16–25 degrees) and heavy load (average blade angle is 35–42 degrees) is significantly different. The operation of heavily loaded propellers is accompanied by the formation of stall zones, large vortex ropes and an increased noise level, one of the sources of which is the vortices formed in the area where the blades adjoin the inner surface of the duct. The existence of these vortices is observed on any airfoil of finite size. At the same time, the presence of separated vortex flows is not always a negative factor from the point of view of the influence on the aerodynamics of the object, which does not make it possible to unambiguously assess the nature of their interaction with complex propulsion structures.

Since the operation of propellers under heavy and moderate loads in the swept area differs, there is a need to investigate the applicability of different turbulence models depending on UAV operating mode. At an installation angle of the blade of 75% of its length in the range from 20 to 25 degrees, standard turbulence models such as Spalart–Allmaras and SST give approximately the same result as the $\gamma$–$\mathrm{Re}_{\theta t}$ model, which takes into account laminar-turbulence transition [30].

In the clearance between the propeller blades and the ducts, a low-Reynolds flow occurs from the bottom surface of the airfoil blade to the top one. This phenomenon is accompanied by the formation of vortical ropes at the tip of the blades. The parameters of these tip vorticies and their impact on the aerodynamics of the propulsive system itself depend upon numerous factors.

One of the most important one is the size of the clearance between the blade tip and the duct. This clearance acts as a vortex cell that determines the characteristics of vortical flow. It is important to study the influence of the tip clearance on aerodynamic characteristics and vortical structure of flow. In this case, it is necessary to take into account the presence of low-Reynolds air flow through the tip clearance and extensive zone of laminar flow on the front side of the highly loaded blades, which requires the use of turbulence models that take into account the laminar-turbulent transition.

One of the most important factors is the size of the gap between the blade's tip and the air duct. This gap acts as a vortical cell that determines the properties of the vortical airflow. It is essential to study how the tip gap affects the aerodynamic properties and vorticial structure of the flow. In such cases, it is crucial to consider the presence of a low-Reynolds number airflow through the tip gap and an extensive region of laminar airflow on the leading edge of highly loaded blades. This requires the use of turbulent models that account for the laminar-turbulent transition of flow.

In this study, aerodynamic and thrust characteristics of a ducted fan were assessed over a wide range of parameters using the full Navier-Stokes equations written in a rotating coordinate system and modern approaches for simulating turbulent flows. The effect of clearance between blade tips and the inner wall of ducts on thrust and power was investigated.

 doi:10.20944/preprints202603.2079.v1



## 2. Materials and Methods

### *2.1. Geometric Model*

For UAV design, highly loaded VK1-K184V propellers are considered using an air duct representing a body of rotation with an aerodynamic airfoil in cross-section. The use of an air duct in conditions of low propeller speed (low speed of the flow incident on the propeller) allows to increase the mass flow rate of air passing through the duct increasing thrust by creating air circulation around the airfoil of the duct and reduce the power on the propeller. The flow pattern around a propeller ring largely depends on its geometric parameters.

The parameters of the geometric model of a blade are set based on an analysis of open sources. Graphs from [1] were used to profile fan blades. The distribution of relative blade thickness $c$ and curvature $f$ is shown in the graphs, as well as the rotation angle $\varphi$ and the chord length $b$ of the blade along the relative propeller radius (the radius of the section plane divided by the total propeller radius). The air duct VK1 was modelled based on known relationships reported in [1]. The geometric parameters for the fan were found from the K6 - VK1 geometry of a four-bladed ducted fan with a 25% reduction in air duct length. The duct diameter was 760 cm [2].

The design of a ducted fan consists of a heavily-loaded propeller (2), and an airduct (1), formed by the rotation of an airfoil. A ducted fan can be seen in Figure 1, where the $x$-axis of the cartesian frame of reference is aligned with the direction of free-stream airflow. The angle of deviation $\gamma$ of the airfoils from the vertical is a model parameter.

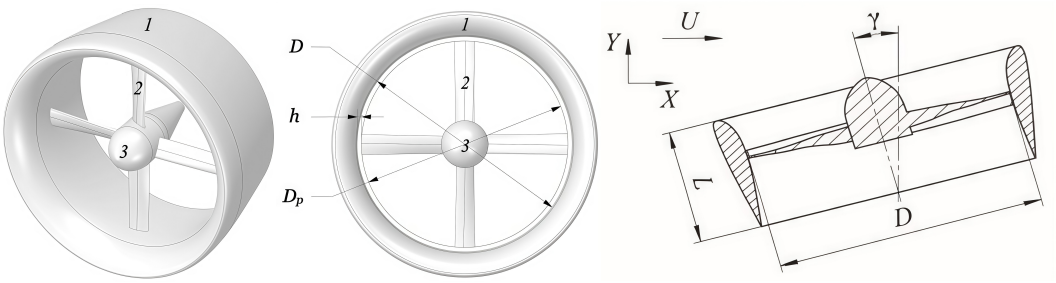


**Figure 1.** Model of a four-blade fan with a hub (a), its geometric characteristics (b and c) (1 is duct, 2 is blade, 3 is fan hub, $D$ is inner diameter of the duct, $D_p$ is outer diameter of blade, $h$ is clearance between blade tip and duct).

To increase thrust at low speeds and reduce tip loss when operating in ducts, the blade shape is rectangular. These blades have lower torsional stiffness compared to elliptical ones, so they are not suited for aircraft propeller applications due to the risk of stall flutter. In order to increase torsional stiffness, a larger relative thickness c is chosen, but this is not suitable for propellers because of large wave loss in cruise mode. The chosen thickness, curvature, and shape of airfoils provide high lift coefficients and delay separation. This, combined with a larger thickness, avoids stall flutter, allowing for a rectangular-shaped blade.

For the K164 propeller, in the peripheral sections of the blade with $c \ll 12\%$, it was possible to accept an airfoil curvature of $f = 7\%$, which ensured continuous flow with high lift coefficients. At the root of the blades, with values of $c > 12\%$ the curvature decreased, since a large relative thickness at the root section led to a larger curvature and an earlier separation of the flow.

The blade twist angle varies from 10 degrees near the hub to ˜7.5 degrees at the tip of the blade, which is much less than the typical twist angle found in propellers. This particular propeller has been designed for use at low speeds. The distribution of geometric parameters across the height is shown in Figure 2.

 doi:10.20944/preprints202603.2079.v1



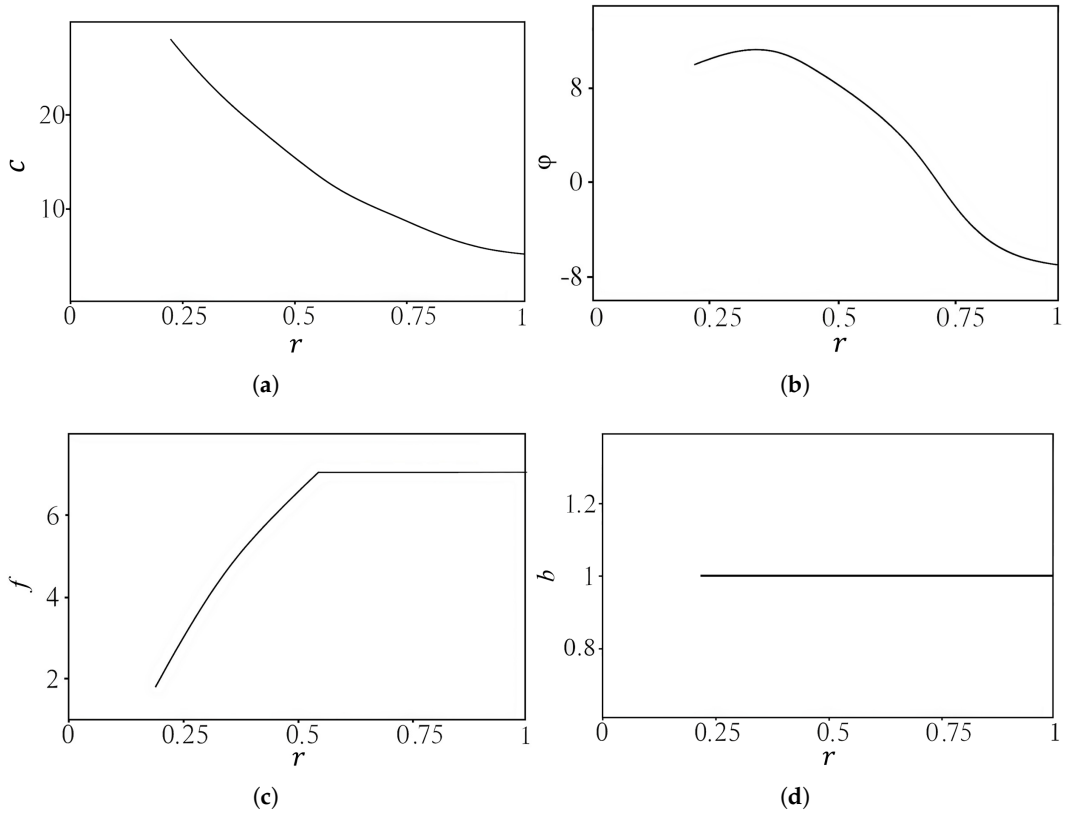


**Figure 2.** Geometric parameters of the blade ($c$ is relative thickness of airfoil, $\varphi$ is twist of blade, $f$ is relative curvature of airfoil, $b$ is relative width of propeller blade).

The duct in a ducted fan is a rotating body with an aerodynamic airfoil in cross-section. It increases speed through the propeller inlet, reduces radial leakage, enhances thrust, and decreases blade moment. Key duct parameters include a relative width of $b_k/D_k = 0.6$, with $D_k$ being the smallest diameter; a maximum relative thickness of $c_k/b_k = 18\%$; maximum relative curvature of $f = 4\%$; and a chord angle of $\gamma = -7^\circ$ to the axis of rotation. The blade rotation plane is positioned $\lambda_v = 0.1b_k$ from the duct's leading edge. Duct opening coefficient is $F_1 = D_1^2/D_k^2 = 1.45$ and expansion coefficient is $F_2 = D_k^2/D_2^2 = 1.1$, where $D_1$ and $D_2$ are the diameters of the inlet and outlet sections of duct. The overall diameter of duct is 26% larger than the diameter of blade.

### *2.2. Mathematical Model and Boundary Conditions*

To simulate the flow induced by fan blades, full Navier–Stokes equations are used for calculations. These calculations are carried out in order to find stationary and non-stationary flow fields, and to determine aerodynamic loads and trust characteristics of the fan blades. Turbulent flow modelling is carried out using unsteady Reynold-averaged Navie–Stokes equation and SST (Shear Stress Transport) turbulence model. Air is the working substance, and its density varies according to an ideal gas model, while its viscosity is constant.

The speed and total temperature are specified at the inlet boundary of computational domain, and the static pressure is fixed at the remaining boundaries. The intensity of turbulence at the inlet boundary is 5%, and the ratio between turbulent viscosity and laminar viscosity for air is 10. No-slip and no-penetration boundary conditions are applied to the walls. Adiabatic boundary conditions are specified on the walls.

The simulation is performed on a unstructured mesh composed of tetrahedral elements. The total number of elements is 3 million, and the maximum element size in the main part of the domain is 0.1 meters. A portion of the mesh containing prismatic elements adjoins solid walls, with a thickness of 1 millimeter, 5 layers, and a cell growth factor of 1.2.

 doi:10.20944/preprints202603.2079.v1



The geometric model of a ducted fan consists of a flow duct and rotating parts. The computational domain consists of rotating (rotor) and stationary sub-domains (stator). To take into account the interaction between rotating and stationary domains, the sliding mesh technique is used. The rotor and surrounding elements of the device are calculated in a rotating coordinate system and the rest is calculated in a stationary one. The boundary of the partition is not a structural part of the device but an auxiliary rotating surface that divides the mesh into several sections. The mesh does not move when the position of a rotating body changes, as the mesh rotates with the moving parts.

To accelerate convergence, a non-zero initial distribution of velocities and pressures is specified. A frozen rotor model is used to determine the initial distribution of fluid quantities on a fine mesh. In this frozen rotor approximation, geometry is frozen in a specific position, allowing one to study flow fields for a selected position of the rotor (the blades remain stationary relative to the channel, and centrifugal forces act on the surrounding area). Using a frozen rotor approach, updating the location of the rotating grid relative to the static one is also deactivated, reducing the computational time per iteration.

### *2.3. Numerical Method*

To discretize the governing equations, the finite volume method on unstructured grids and the median control volume are used [31]. Integration over time is performed using the 3rd-order Runge–Kutta method. Discretization of inviscid flows is performed using the MUSCL (Monotonic Upstream Schemes for Conservation Laws) scheme, while viscous flows are discretized using a centered scheme with second-order accuracy. The MUSCL scheme allows for increasing the order of spatial approximation without losing monotonicity in the solution, satisfying the TVD (Total Variation Diminishing) condition, and combining centered finite differences with a dissipative term of second order. To switch between which a flux limiter designed with characteristic variables is used. Finding the gradient and the pseudo-Laplace operator at the mid-point of a control volume face based on relations that are adapted for calculations in highly stretched cells in the boundary layer is used to solve a system of finite-difference equations. A geometric multigrid technique is used for this purpose. A sequence of grids with different resolutions is generated using the edge-collapsing method.

The results of numerical modeling are the pressure and velocity fields, both in the computational domain and directly on the blade surface, which allows us to determine the aerodynamic properties of the propulsive system in different modes. The thrust force created by the fan blades $P_1$, the thrust force created due to circulation around the airfoil of the duct $P_2$, the drag force of the propeller hub $P_3$, the moment of resistance to rotation $M$ are determined. The resulting force makes it possible to determine the total thrust of a given ducted fan as $P = P_1 + P_2 - P_3$. The thrust coefficient is found as $\alpha = P/\rho n^2 D^4$, and the power coefficient is calculated as $\beta = N/\rho n^3 D^5$, where $\rho$ is air density, $D$ is blade diameter, $P$ is thrust force. The required power on the shaft is determined as $N = 2\pi n M/60$ [W], where $n$ is rotation speed [rpm], $M$ is moment of resistance to rotation [N m].

### *2.4. Turbulence Model*

Two series of calculations are carried out with SA and STT turbulence models proposed in [33,34], and with $\gamma$–$\mathrm{Re}_{\theta t}$ turbulence model taking into account the laminar-turbulent transition [35,36]. In $\gamma$–$\mathrm{Re}_{\theta t}$ model, the boundary layer is divided into sections of laminar ($\gamma = 0$), transition ($0 < \gamma < 1$) and turbulent ($\gamma = 1$) flows depending on intermittency parameter.

In calculations, the angle of installation of fan blades is varied, and graphs of the dependence of thrust coefficient on power coefficient are plotted, which are compared with experimental data. The variable parameter is the angle of installation of the blade. The rotation speed remains constant and equal to 1200 rpm. The oncoming flow velocity is 0.05 m/s. The direction of the oncoming flow is axial. The Reynolds number at the periphery of the blade is $\mathrm{Re} = ub/\nu$, where $u$ is the peripheral speed, $b$ is the chord, $\nu$ is the kinematic viscosity. For the given conditions, $\mathrm{Re} = 2.9 \times 10^6$.

The limiting streamlines on blade surface make it possible to evaluate the nature of flow around the elements of ducted fan and type of flow behind it. Streamlines and pressure contours at installation

 doi:10.20944/preprints202603.2079.v1



angles of 5, 30 and 40 degrees are presented in Figures 3 and 4. At an installation angle of 40 degrees, when using the SST model, a vortex appears on the front surface near the periphery, which causes a sharp drop in the dimensionless coefficients. At smaller angles, there is a slight shear from the front surface near the trailing edge, and it becomes more pronounced as the installation angle increases.

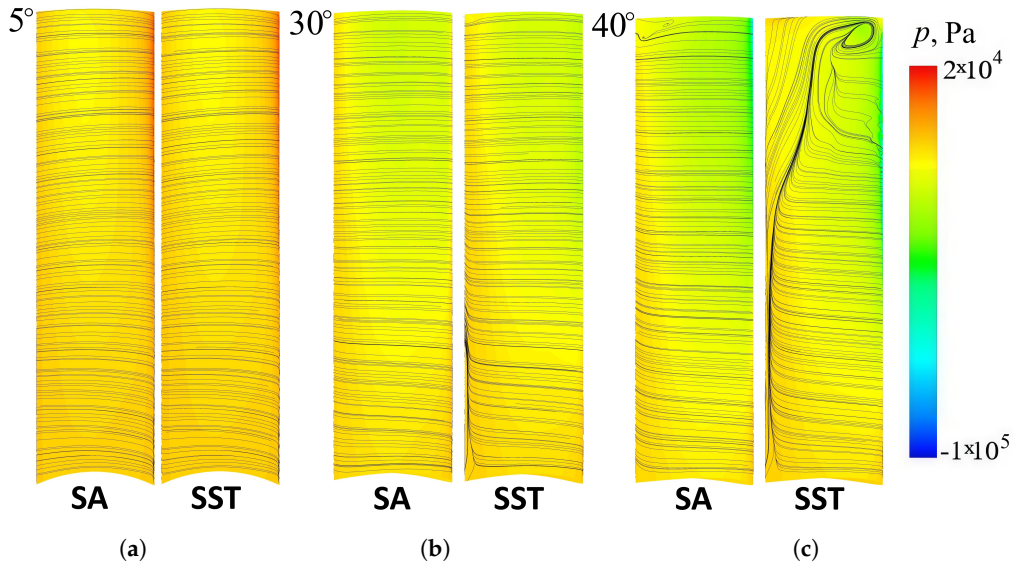


**Figure 3.** Streamlines and pressure contours on upstream surface of blade.

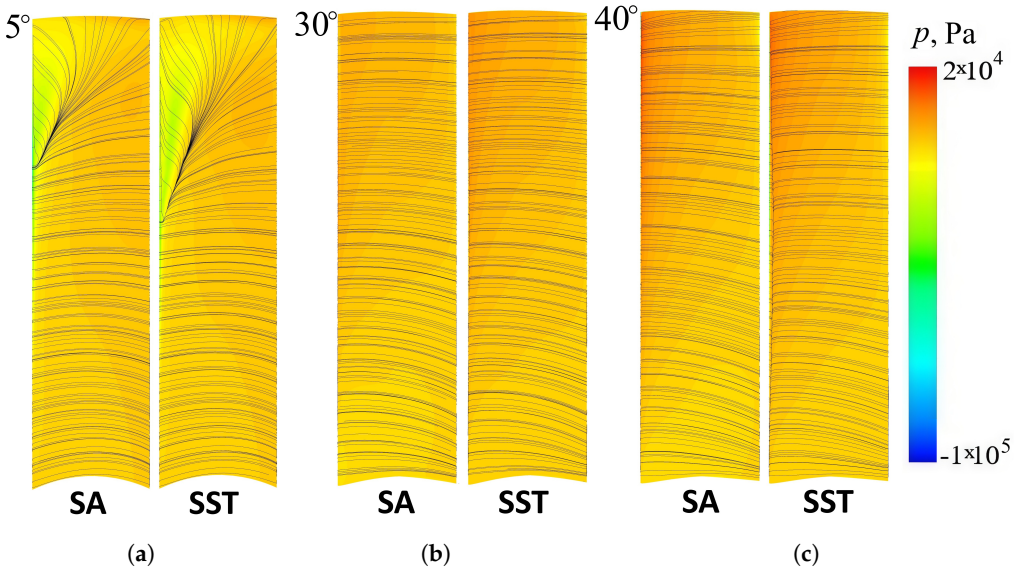


**Figure 4.** Streamlines and pressure contours on downstream surface of blade.

 doi:10.20944/preprints202603.2079.v1



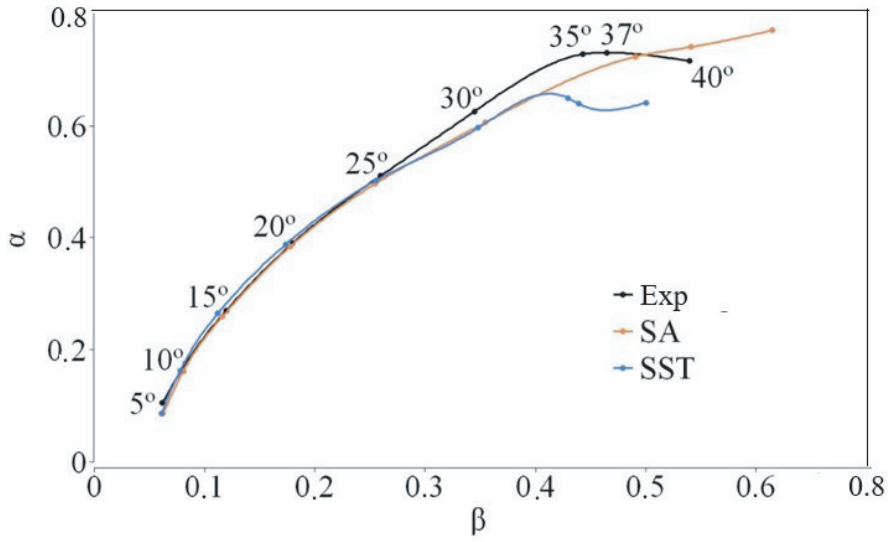


**Figure 5.** Dependencies of thrust and power characteristics.

## 3. Results

### *3.1. Effect of Blade Angle*

The calculation of the flow around a ducted fan, with optimal angles for the installation of fan blades relative to oncoming flow, is carried out. The oncoming flow speed varies from 25 to 75 m/s. For each value of oncoming flow velocity, the optimal rotation angle of fan blade is calculated (60.64 degrees at $U = 25$ m/s, 74.29 degrees at $U = 50$ m/s, 79.38 degrees at $U = 75$ m/s). The angle of deviation of blade from the vertical is 15, 30 and 45 degrees. The duct length is $L = 337$ mm.

Streamlines at different free flow velocities and angles of deflection of the ducted fan from the vertical are shown in Figure 6. In the flow in front of the blade, the streamlines are directed along the axis of rotation into the duct, resulting in the effect of suction of free air into the duct. In this case, the velocity decreases along the radius of the duct and becomes negligible on the outer surface. Behind the blade there is a significant acceleration of the axial flow velocity on a cylindrical surface on order of radius of duct and its twisting, co-directed with the direction of rotation of the blade. As the radius decreases and the distance increases, the axial velocity decreases and, as a consequence, the amount of flow swirl increases. Behind the central body, where the axial velocity is practically zero, the streamlines are twisted into a bundle. In the lower part of flow, in the vicinity of the rotation axis, spiral vortices are formed.

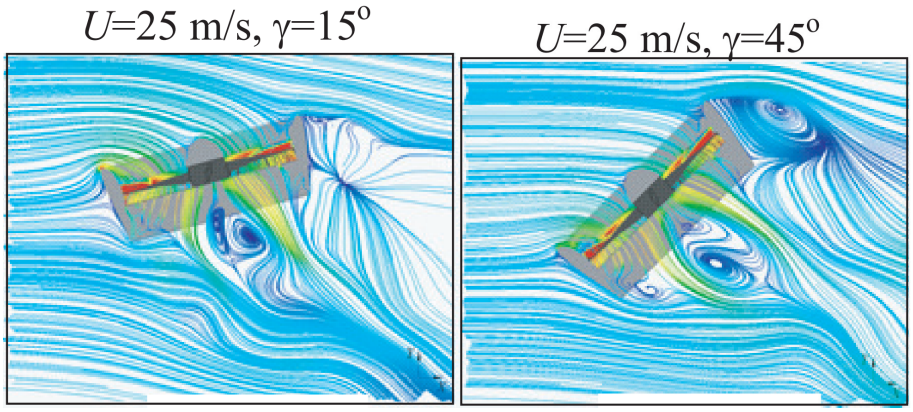


(**a**) (**b**)

**Figure 6.** *Cont.*

 doi:10.20944/preprints202603.2079.v1



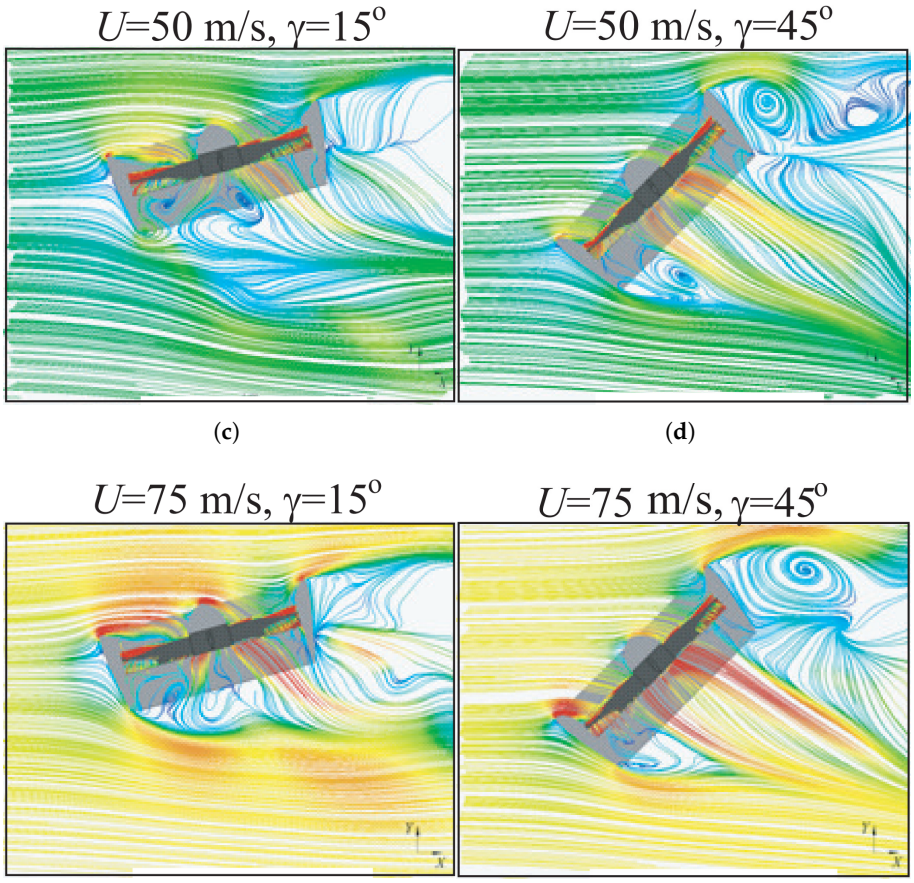


**Figure 6.** Influence of velocity in outlet section of duct and angle of deviation from vertical on streamlines.

In front of blades and to the side of it there is a suction zone, the flow speed in which increases as it approaches the blades. The intensity of flow decreases as it approaches the axis of rotation of the blade, where low-speed turbulent structures are observed near the butt parts of the blades. Behind the fan, the flow velocity reaches its maximum in the cone below the blade tips and decreases further downstream from the fan. The most intense turbulent structures are tip vortices coming off the blade tips and twisting into characteristic tapering spirals descending downstream from the plane of rotation of the fan. With distance from the rotor disk downstream, the intensity of turbulent structures decreases.

The distributions of axial and circumferential velocities in the outlet section of the duct at different incoming flow velocities and angle of deviation of the ducted fan from the vertical are shown in Figures 7 and 8.

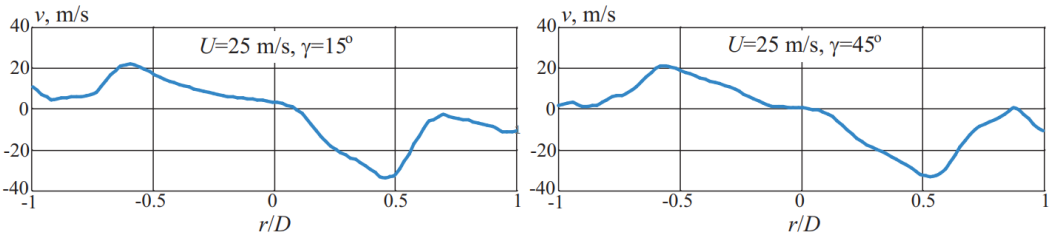


**Figure 7.** *Cont.*

 doi:10.20944/preprints202603.2079.v1



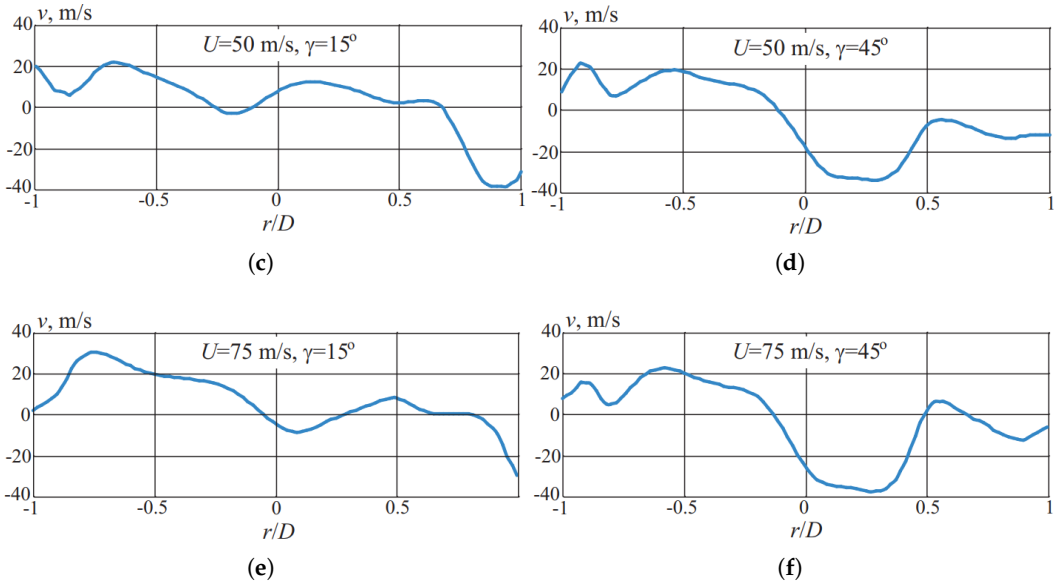


**Figure 7.** Influence of velocity in outlet section of duct and angle of deviation from the vertical on distribution of axial velocity.

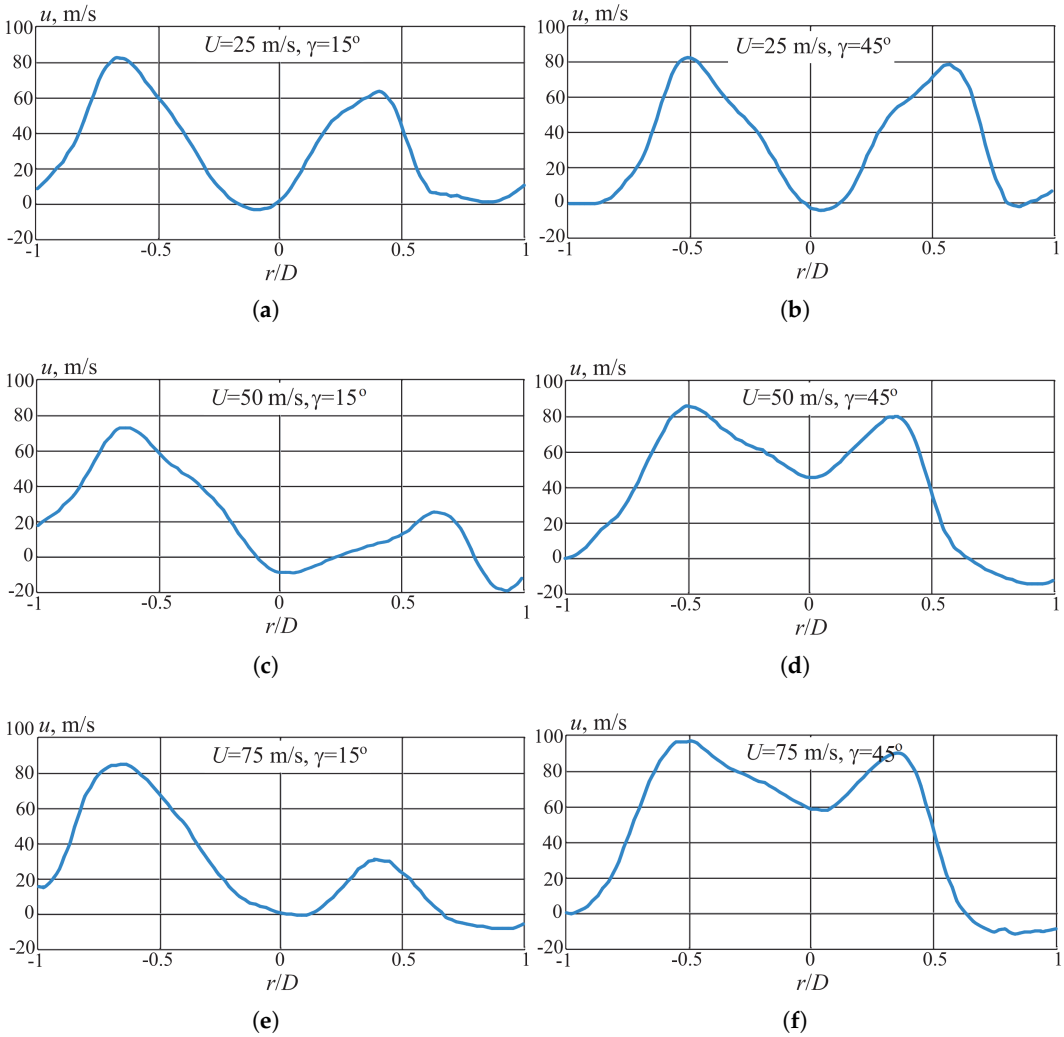


**Figure 8.** Influence of velocity in outlet section of duct and angle of deviation from the vertical on distribution of circumferential velocity.

 doi:10.20944/preprints202603.2079.v1



The influence of the speed and angle of deviation of blade from the vertical on the thrust characteristics is shown in Figure 9.

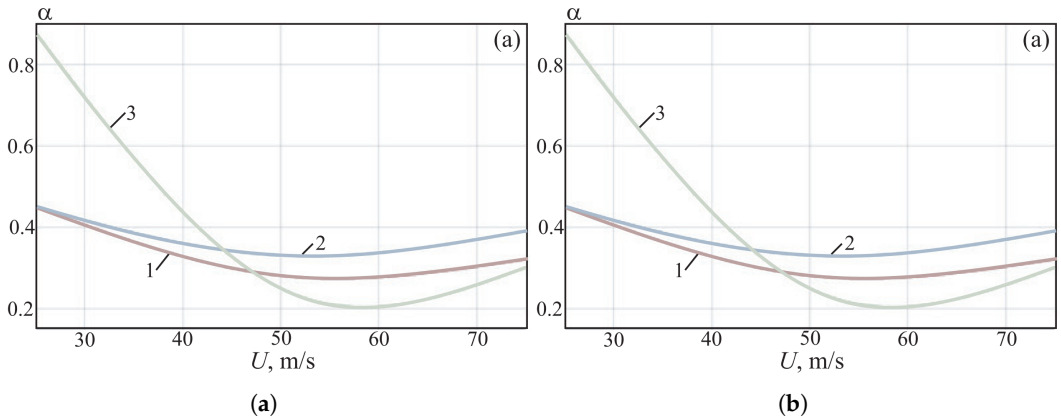


**Figure 9.** Dependence of thrust coefficient (a) and power coefficient (b) on free-stream speed for various angles of deviation from the vertical $\gamma = 15^c irc$ (1), $30^c irc$ (2), $45^c irc$ (3).

The results obtained show both the change in the total thrust force coefficient and change in its components (fan thrust force and duct thrust force) depending on speed of oncoming flow and angles of deflection of ducted fan from the vertical. The forces acting on the ducted fan and its elements for various velocities of oncoming flow and angles of deviation of ducted fan from the vertical are shown in Figure 10. The relative thrust coefficient of fan is a small value of the total thrust. The high load capacity is associated with the optimal configuration of duct, which has a relatively large radius of curvature of the collector, and a sufficiently long diffuser [9].

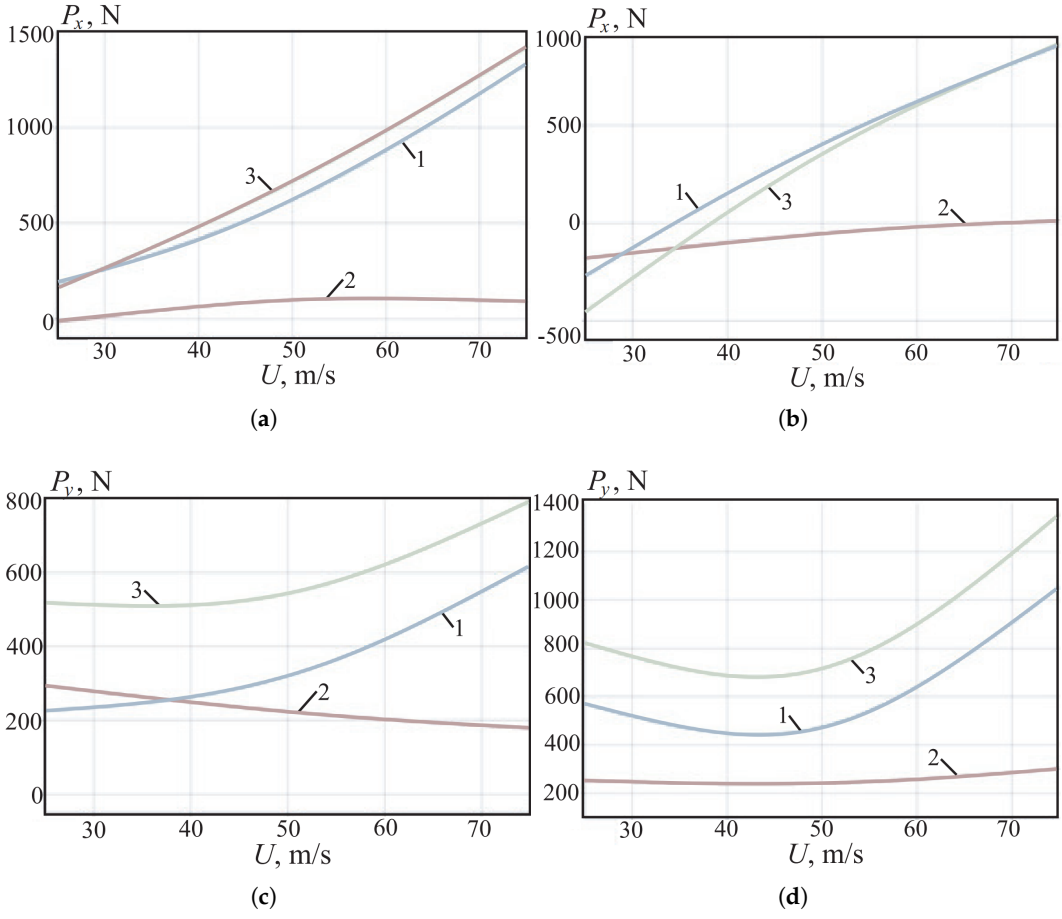


**Figure 10.** Dependencies of thrust forces on $x$ and $y$ axes on free flow velocity at $\gamma = 15^c irc$ (a, c), $45^c irc$ (b, d) for duct (1), fan (2), duct and fan (3).

 doi:10.20944/preprints202603.2079.v1



The total thrust coefficient and the thrust coefficient of fan at zero angle of attack increase with increasing speed due to an increase in mass flow of air passing through the fan. When the angle of deflection of blade from the vertical changes, the total thrust decreases significantly due to a drop in the thrust of the duct.

### 3.2. Effect of Tip Clearance

In the tip between the fan blade and the aerodynamic duct, a low-Reynolds flow occurs from the lower surface of the blade to the upper surface (flow is laminar). Fan blades exhibit an extensive laminar boundary layer zone on the downwind side. Rotation of a fan in the presence of a tip is accompanied by the formation of vortex ropes of different sizes and intensity at the blade tips.

The size of the internal diameter of the air duct in each of the considered cases remains unchanged due to the need to maintain the air mass flow rate for a relevant comparison of the thrust characteristics. Changing the tip clearance $h$ is achieved by slightly reducing the length of the blade. The influence of the tip clearance is studied within its relative value $h/D$ equal to 0.02, 0.015, 0.008 and 0. In the absence of a tip clearance ($h = 0$), it is assumed that the fan blades are embedded in the inner surface of the air duct and rotate together with the annular segment of this surface. Calculations are carried out for blade installation angles of 16 and 32 degrees. The section relative to which the angle of installation of blade is set, is located at 75% of its length.

Table 1 shows the results of calculations demonstrating the influence of the clearance size on thrust, torque and power on the shaft, and dimensionless thrust and power coefficients.

**Table 1.** Results of calculations of traction characteristics depending on the size of the gap blade installation angle, degrees.

| Angle, deg | Clearance $h/D$, % | $\alpha$ | $\beta$ | $M$, N m | $N$, W | $P$, N |
|---|---|---|---|---|---|---|
| 16 | 0 | 0.2684 | 0.1802 | 5.672 | 1782 | 91.48 |
| 16 | 0.8 | 0.2623 | 0.1353 | 4.258 | 1338 | 89.44 |
| 16 | 1.5 | 0.2616 | 0.1299 | 4.089 | 1284 | 89.17 |
| 16 | 2 | 0.2478 | 0.1355 | 4.264 | 1340 | 84.47 |
| 32 | 0 | 0.8406 | 0.5042 | 15.867 | 5051 | 286.56 |
| 32 | 0.8 | 0.7016 | 0.3851 | 12.119 | 3838 | 239.17 |
| 32 | 1.5 | 0.6199 | 0.4418 | 13.905 | 4368 | 211.32 |
| 32 | 2 | 0.5940 | 0.4196 | 13.203 | 4148 | 202.51 |

At both blade installation angles, as the clearance increases, the thrust force decreases almost monotonically. This is due to flow of part of oncoming flow through the clearance between the blade tip and inner surface of duct, avoiding interaction of air flow with working surfaces of blades, and a reduction in area of working surface of blades due to addition of a clearance. In this case, a change in flow structure associated with formation of tip vortices at the blade tips also makes a contribution. They have a particular influence on amount of power required to drive and rotate the fan at a given speed, since the appearance of separated vortex flows of different configurations leads to a significant redistribution of pressure and change in size and position of characteristic flow zones on working surface of blade.

An assessment of aerodynamic characteristics when using a finite power power fan is carried out. To do this, after obtaining the dimensionless characteristics, the fan rotation speed is changed to values that can be achieved for the target power value. The value $N = 3750$ W per propulsion unit is taken as such a target value. Table 2 presents the results of a numerical calculation with the reduction of different ducted fan designs to a single power value by changing the rotation speed. At the same time, the values of dimensionless coefficients are preserved (the operating mode that is obtained when changes are made to the design of blade is maintained). If, with a large angle of installation of the blades and a heavy load on the fan, the thrust drops noticeably with increasing clearance, then with

 doi:10.20944/preprints202603.2079.v1



a moderate load the situation is different. The thrusts at clearances $h/D = 0.8$ and 1.5% are almost equal (there is no need to strive to endlessly reduce the clearance), which is technologically difficult. It is interesting that when studying moderately loaded fans with a given shaft power ($N = 3750$ W), the optimal value $h/D = 1.5\%$ is obtained (Table 2).

**Table 2.** Calculation results for a given drive power.

| Angle, deg | Clearance $h/D$, % | $\alpha$ | $\beta$ | $M$, N m | $N$, W | $P$, N |
|---|---|---|---|---|---|---|
| 16 | 0 | 0.2684 | 0.1803 | 3845 | 3750 | 150.28 |
| 16 | 0.8 | 0.2623 | 0.1353 | 4230 | 3750 | 177.81 |
| 16 | 1.5 | 0.2616 | 0.1299 | 4288 | 3750 | 182.17 |
| 16 | 2 | 0.2478 | 0.1355 | 4228 | 3750 | 167.77 |
| 32 | 0 | 0.8406 | 0.5042 | 2728 | 3750 | 236.95 |
| 32 | 0.8 | 0.7016 | 0.3851 | 2985 | 3750 | 236.78 |
| 32 | 1.5 | 0.6199 | 0.4418 | 2851 | 3750 | 190.85 |
| 32 | 2 | 0.5940 | 0.4196 | 2901 | 3750 | 189.37 |

[1] Tables may have a footer.

For heavily loaded fans, thrust drops as expected with increasing clearance (there is no need to reduce the clearance below $h/D = 0.8\%$, since thrust does not increase). There is a certain optimal clearance, the value of which depends on the angle of installation of blades. With an installation angle of 16 degrees and clearance of 1.5%, the thrust is almost the same as with clearance of 0.8%, but the power on the shaft is less. At a given power on the shaft, the blade with a clearance of 1.5% has maximum thrust.

In Figure 11 for an installation angle of 32 degrees and clearance of 2.0% shows streamlines and isosurfaces of $Q$-criterion ($Q = 10^6$). The vortex rope has a strong influence on air flow around the blades. When the clearance is 2%, the flow incident on blade is strongly twisted and entrained in a vortex spiral flow near the walls of air duct. The specific behavior of streamlines is associated with the emergence of intense stable vortex structures. Strongly twisted by the initial region of the vortex flow, the flow is carried to the center of air duct, pressing the core of the vortex and the air flow entrained by it against the walls of duct. Thus, the decay of the vortex flow of the tip vortex is delayed and occurs much later. At the blades there is a transition from laminar flow (irrotational regions) to turbulent flow. The tips of the blades leave behind a turbulent vortex wake. The vortex core has an extension of more than a quarter of the circumference of blade duct.

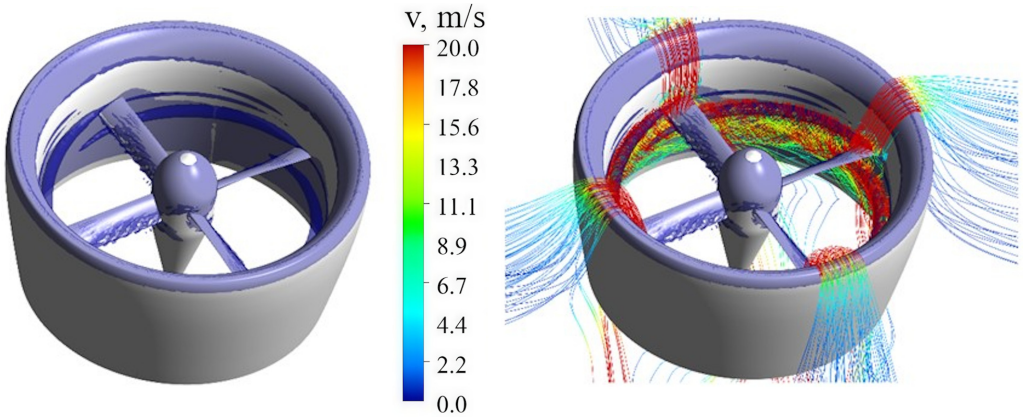


**Figure 11.** Isosurfaces of $Q$-criterion (a) and streamline (b) at a blade angle of 32° and clearance of 2.0%.

An analysis of flow in the vicinity of clearance at a blade angle of 16 degrees shows that thrust losses are simultaneously influenced by two factors, the flow from a high-pressure region to a low-

 doi:10.20944/preprints202603.2079.v1



pressure region and a vortex rope formed in the clearance. The larger the value of $h$, the greater the thrust loss due to overflow. The intensity of eddy losses is affected differently by the clearance size. At small $h$, an intense thin vortex rope is formed, which spreads over a considerable distance and greatly affects the flow behind the fan (Figure 12a). With large clearance, its influence on formation of a vortex is minimal (Figure 12b and c), but the nature of flow inside the duct is such that the vortex is quickly washed out, therefore, usually in the ducted fan the tip losses for vortex formation are less than in isolated fan.

(**a**) (**b**) (**c**)

**Figure 12.** Formation of a vortex rope at the blade tip with clearance of 0.8% (a), 1.5% (b) and 2% (c). Blade installation angle is 16°.

At $h = 0$ inside the air duct, the flow velocity is distributed uniformly. The change in speed is observed in a local area near the surfaces of fan blades. With the appearance of a tip clearance, the formation of a vortex end rope can be observed. With an increase in clearance size, the formation of a wider, due to the increase in the width of the vortex cell, and a short vortex core is observed. Its small length is explained by more intense dissipation of the vortex rope due to an increase in its initial dimensions. Due to the rapid decay of the vortex rope, the flow induced by the rotation of the blades can quietly expand in the expanding segment of the air duct located behind the plane of rotation of fan. This leads to less air deflection when interacting with the blade and the absence of flow separation in the area of the air duct diffuser.

For heavily loaded fans, dependence of the thrust force on $h$ is uncharacteristic. The vortex bundles in this case have transverse dimensions that are significantly larger than the clearance, and a length greater than a quarter of the circle. As a result, the vortices of individual blades feed the vortices of the leading blade, and they merge into one common vortex duct.

At a blade installation angle of 32 degrees (Figure 13), flow separation from the central body is observed, associated with a large angle of inclination of the root section of blade relative to induced flow at a given installation angle. In the axial planes, some inhomogeneity of the velocity field is observed inside the space of the blade air duct. Near the axis of rotation of the blade, a non-uniformity of the velocity field is observed, associated with the general twist of the air flow by the rotating fan. At the wall near the plane of rotation of fan, a local increase in speed is observed, which is associated with a vortex rope formed at the blade tips. As the clearance width increases, the length of the vortex core of the end bundles becomes noticeably smaller and wider in the region of its origin. An increase in the thickness of the vortex jet leads to its rapid dissipation in the surrounding space. At clearance width of 2.0%, significant changes in the flow structure occur. A significant increase in the length of the vortex end rope is observed. The clearance size, acting as a vortex cell, gives rise to wide and intense vortex end ropes. The formation of vortex ropes of similar sizes leads to the interaction of vortex tip wakes from neighboring blades. They push and feed each other, preventing the vortex core from quickly disintegrating into small-scale chaotic turbulence.

 doi:10.20944/preprints202603.2079.v1



(**a**) (**b**) (**c**)

**Figure 13.** Formation of a vortex rope on blade tip at clearance of 0.8% (a), 1.5% (b) and 2.0% (c). Blade installation angle is 32°.

The nature of the change in aerodynamic characteristics at different blade installation angles is different. In fact, the thrust graphs when the fans are brought to a single power value reflect the efficiency of the ducted fan design. At a blade angle of 16 degrees, there is a clear optimum. The absence of a clearance is the least effective mode of the considered design cases, since in the mode of small flow incident on fan and the considered blade rotation speed (3000 rpm), this angle is not optimal from the point of view of angle of flow on blade airfoil. In this regard, a large moment of rotational resistance arises on the fan blades, which, when the slightest tip clearance appears, is significantly reduced, improving the efficiency of the ducted fan. This is associated with a local increase in work efficiency. At the same time, with an increase in the clearance size, the intensity of tip vortex decreases, which, although it increases in size due to an increase in the size clearance, dissipates inside the air duct much faster, reducing its contribution to the resistance to rotation of fan. When the clearance reaches a certain value, the influence of the tip vortex becomes not so significant, however, the thrust force of fan begins to decrease due to a decrease in the length of the working area of the blades, which leads to a general decrease in the efficiency of the blade.

At a blade installation angle of 32 degrees, a slightly different relationship is observed. The angle of flow on blade airfoil is closer to optimal one, therefore, even without the presence of tip clearance, the most efficient operating mode is observed. Despite the significant reduction in thrust without reducing the rotational power to a single power, the clearance also significantly relieves the working surfaces of fan blades, which ultimately leads to the high efficiency of this design. A further increase in the clearance width leads to a deterioration in the efficiency of fan, since such an expansion of the beginning of the vortex core at an installation angle of 32 degrees does not lead to a significant decrease in the intensity of the vortex rope, while the useful area of the working surface of blade decreases. A further increase in the clearance, despite the complex flow pattern, only leads to a decrease in working area of blade, due to which the moment and thrust on blades are reduced, as well as the flow of a noticeable part of the flow through the clearance, due to which the moment of resistance to rotation also decreases (the necessary drive power).

## 4. Discussion

Authors should discuss the results and how they can be interpreted from the perspective of previous studies and of the working hypotheses. The findings and their implications should be discussed in the broadest context possible. Future research directions may also be highlighted.

The computational results obtained using SA, SST and $\gamma$–$\mathrm{Re}_{\theta t}$ turbulence models are compared. The SA model does not capture separation at the downstream surface of blade. The SST model takes into account the effect of increased thrust due to the separation bubble and, as a consequence, an increase in the effective airfoil thickness. Moreover, both models are applicable to angles of attack without separated flow (for the model blade, this range is from 0 to 25 degrees). Inside the ducted fan, on the surface of the duct and blades, there are vast areas with laminar flow, so in calculations it is

 doi:10.20944/preprints202603.2079.v1



necessary to use methods that take into account the laminar-turbulent transition. The use of the $\gamma$–$\mathrm{Re}_{\theta t}$ model is required in the clearance between fan blade and duct, where low-speed flow from the lower surface of blade to upper one is observed.

A study of dependence of operation of a ducted fan on clearance size shows that there is a complex interaction between the flow in the slot and the tip vortices of fan blades. With a moderate load on the fan and an installation angle of the blades of 16 degrees, the optimal clearance is found. It does not make sense to reduce, because this does not lead to increased thrust. For the fan considered, this optimal value is equal to 1.5% of the fan diameter. The reason for the presence of an optimum lies in the multi-directional effect of increasing the clearance on thrust loss. On the one hand, an increase in the clearance leads to an increase in thrust losses due to the flow from high pressure region to low pressure one.With a moderate load on the fan and small clearances, a thin intense vortex is formed, which is slowly eroded by the flow behind the fan, which causes increased vortex losses.

Vortex ropes are formed at the blade tips, the unsteady interaction of which with the underlying surface is important when considering the landing mode of the quadcopter.

**Author Contributions:** Conceptualization, P. Bulat; methodology, P. Bulat; software, P. Bulat; validation, P. Bulat; formal analysis, P. Chernyshov; investigation, P. Chernyshov; writing—original draft preparation, P. Chernyshov; writing—review and editing, P. Chernyshov; visualization, P.Chernyshov; supervision, P. Bulat; project administration, P. Bulat. All authors have read and agreed to the published version of the manuscript.

**Funding:** This work was financially supported by the Ministry of Science and Higher Education of Russian Federation during the implementation of he project «Fundamentals of aerodynamics, flight dynamics and control of transport unmanned aerial systems of a new generation with a distributed propulsion system», № FEFM-2024-0012.

**Informed Consent Statement:** Not applicable.

**Conflicts of Interest:** The author declares no conflict of interest.

## Abbreviations

The following abbreviations are used in this manuscript:

| | |
|---|---|
| UAV | Unmanned Aerial Vehicle |
| RANS | Reynolds-averaged Navier–Stokes model |
| URANS | Unsteady Reynolds-averaged Navier–Stokes model |
| DES | Detached Eddy Simulation model |
| SST | Shear Stress Transport model |
| MUSCL | Monotonic Upstream Schemes for Conservation Laws |
| TVD | Total Variation Diminishing |
| SA | Spalart–Allmaras model |

## References

1. Ostroukhov, S.P. *Aerodynamics of propellers and propeller rings*. Moscow: Fizmatlit, 2014.
2. Buzykin, O.G.; Kazakov, A.V.; Shustov, A.V. Numerical modeling of the aerodynamic characteristics of a small-sized aircraft. *Scientific Notes of TsAGI* **2010**, *51*, 21–31.
3. Czyba R.; Szafranski G. Control structure impact on the flying performance of the multi-rotor VTOL platform — design, analysis and experimental validation. *International Journal of Advanced Robotic Systems* **2012**, *10*, 1–9.
4. Hrishikeshavan, V.; Chopra, I. Performance, flight testing of shrounded rotor micro air vehicle in edgewise gusts. *Journal of Aircraft* **2012**, *49*, 193–205.
5. Nazarov, D.V.; Kondryakova, A.V. Study of flow around a propeller using numerical and experimental methods. *Bulletin of the Samara Scientific Center of Russian Academy of Sciences* **2018**, *20*, 70–75.
6. Chovancova, A.; Fico, T.; Chovanec, L.; Hubinsky, P. Mathematical modelling and parameter identification of quadrotor (a survey). *Procedia Engineering* **2014**, *96*, 172–181.

 doi:10.20944/preprints202603.2079.v1




7. Xiang, X.; Huang, G.; Chen, J.; Li, L.; Lu, W. Numerical investigations of a tip turbine aerodynamic design in a propulsion system for VTO vehicles. *Energies* **2019**, *12*, 3003.
8. Golovkin, M.A.; Kocish, S.I.; Kritsky, B.S. Methodology for calculating the aerodynamic characteristics of the combined load-bearing system of an aircraft. *Proceedings of Moscow Aviation Institute* **2012**, *55*, 1–16.
9. Moizykh, E.I.; Zavalov, O.A.; Kuznetsov, A.V. Experimental studies of the aerodynamic characteristics of a remotely piloted aircraft with a rotor-in-a-ring support system. *Proceedings of Moscow Aviation Institute* **2012**, *50*, 1–13.
10. Akturk, A.; Shavalikul, A.; Camci, C. PIV measurements and computational study of a 5-inch ducted fan for V/STOL UAV applications. *AIAA Paper* **2009**, *2009-332*.
11. Akturk, A.; Camci, C. Experimental and computational assessment of a ducted-fan rotor flow model. *Journal of Aircraft* **2012**, *49*, 885–897.
12. Yilmaz, S.; Erdem, D.; Kavsaoglu, M. Effects of duct shape on a ducted propeller performance. *AIAA Paper* **2013**, *2013-0803*.
13. Akturk, A.; Camci, C. Tip clearance investigation of a ducted fan used in VTOL unmanned aerial vehicles. Part I. Baseline experiments and computational validation. *Journal of Turbomachinery* **2014**, *136*, 021004.
14. Garipova, L.I.; Batrakov, A.S.; Kusyumov, A.N.; Mikhailov, S.A.; Barakos D. Determination of aerodynamic characteristics of the main rotor model in the axial flow mode. *Russian Aeronautics* **2014**, *3*, 7–13.
15. Biava, M.; Barakos, G.N. Optimisation of ducted propellers for hybrid air vehicles using high-fidelity CFD. *The Aeronautical Journal* **2016**, *120*, 16321657.
16. Chen, J.; Li, L.; Huang, G.; Xiang, X. Numerical investigations of ducted fan aerodynamic performance with tip-jet. *Aerospace Science and Technology* **2018**, *78*, 510–521.
17. Xu, H.-Y.; Xing, S.-L.; Ye, Z.-Y. Numerical study of ducted-fan lip stall suppression based on inflatable leading lip cell. *Procedia Engineering* **2015**, *126*, 158–162.
18. Ohanian,O.J.; Karni, E.D.; Londenberg, W.K.; Gelhausen, P.A.; Inman, D.J. Ducted-fan force and moment control via steady and synthetic jets. *Journal of Aircraft* **2011**, *48*, 514–526.
19. Zhang, T.; Barakos, G.N. Review on ducted fans for compound rotorcraft. *The Aeronautical Journal* **2020**, *124*, 941–974.
20. Diisi, F.; Barakos, J.; Kusyumov, A.N.; Kusyumov, S.A.; Mikhailov, S.A. DES modeling of flow around a helicopter rotor. *Russian Aeronautics* **2018**, *1*, 40–46.
21. Rumsey, C.L.; Biedron, R.; Farassat, F.; Spence, P. Ducted-fan engine acoustic predictions using a Navier-Stokes code. *Journal of Sound and Vibration* **1998**, *213*, 643–664.
22. Reboul, G.; Polacsek, C.; Lewy, S.; Heib, S. Aeroacoustic computation of ducted-fan broadband noise using LES data. *Journal of Acoustic Society of America* **2008**, *123*, 3539–3539.
23. Rhee, W.; Myers, L.; Mclaughlin, D. Aeroacoustics of vertical lift ducted rotors. *AIAA Paper* **2009**, *2009-3333*.
24. Astley, R.; Sugimoto, R.; Achunche, I.; Kewin, M.; Mustafi, P.; Deane, E. A review of CAA for fan duct propagation and radiation, with application to liner optimisation. *Procedia Engineering* **2010**, *6*, 143–152.
25. Malgoezar, A.M.; Vieira, A.; Snellen, M.; Simons, D.G.; Veldhuis, L.L. Experimental characterization of noise radiation from a ducted propeller of an unmanned aerial vehicle. *International Journal of Aeroacoustics* **2019**, *18*, 372–391.
26. Denisenko, P.V.; Chernyshov, P.S.; Volkov, K.N.; Vokin, L.O. Numerical simulation of the flow around the ducted fan of a quadcopter and determination of its thrust characteristics in various flight modes. *Russian Aeronautics* **2021**, *64*, 224-232.
27. Denisenko, P.V.; Bulat, P.V.; Chernyshov, P.S.; Volkov, K.N. Aeroacoustic characteristics of the quadcopter propulsion system in vertical take-off and landing mode. *Russian Aeronautics* **2021**, *64*, 661-669.
28. Rybakov, D.V.; Chernyshov, P.S.; Vokin, L.O.; Prodan, N.V. Numerical modeling of vertical landing of an unmanned aerial vehicle with rotor-ring propulsors using eddy-resolving methods. *Russian Aeronautics* **2020**, *4*, 197–200.
29. Dudnikov, S.Yu.; Bulat, M.P.; Vokin, L.O.; Kuznetsov, P.N.; Chernyshov, P.S. Mathematical and computer modeling of single-row and double-row six-blade propeller-ring propulsors. *Scientific and Technical Bulletin of Onformation Technologies, Mechanics and Optics* **2022**, *22*, 1226–1236.
30. Bulat, P.V.; Prodan, N.V.; Vokin, L.O. Comparison of turbulence models when calculating model VKD. *Russian Aeronautics* **2022**, *4*, 11–21.
31. Volkov, K. Numerical analysis of Navier-Stokes equations on unstructured meshes / Handbook on Navier-Stokes Equations: Theory and Analysis. Nova Science, 2016, 365–442.

 doi:10.20944/preprints202603.2079.v1




32. Volkov, K. Multigrid and preconditioning techniques in CFD applications / CFD Techniques and Thermo-Mechanics Applications. Springer International Publishing, 2018, 83–149.
33. Spalart, P.R.; Allmaras, S.R. A one-equation turbulence model for aerodynamic flows. *AIAA Paper* **1992**, *1992-0439*.
34. Menter, F.R. Zonal two-equation $k$–$\omega$ turbulence models for aerodynamic flows. *AIAA Paper* **1993**, *93-2906*.
35. Menter, F.R.; Langtry, R.; Volker, S. Transition modelling for general purpose CFD codes. *Flow, Turbulence and Combustion* **2006**, *77*, 277–303.
36. Malan, P.; Suluksna, K.; Juntasaro, E. Calibrating the gamma-Re_theta transition model for commercial CFD, *AIAA Paper* **2009**, *2009-1142*.